Augmented reality visualisation for orthopaedic surgical guidance with pre- and intra-operative multimodal image data fusion

Houssam El-Hariri[1] ✉, *Prashant Pandey*[2], *Antony J. Hodgson*[3], *Rafeef Garbi*[4]

[1]*Biomedical Engineering, University of British Columbia, x421-2366 Main Mall, Vancouver, BC, Canada*
[2]*Biomedical Engineering, University of British Columbia, 2635 Laurel Street, Vancouver, BC, Canada*
[3]*Mechanical Engineering, University of British Columbia, 2345 East Mall, Vancouver, BC, Canada*
[4]*Electrical and Computer Engineering, University of British Columbia, 2332 Main Mall, Vancouver, BC, Canada*
✉ *E-mail: houssam@ece.ubc.ca*

Published in Healthcare Technology Letters; Received on 13th August 2018; Accepted on 20th August 2018

Augmented reality (AR) has proven to be a useful, exciting technology in several areas of healthcare. AR may especially enhance the operator's experience in minimally invasive surgical applications by providing more intuitive and naturally immersive visualisation in those procedures which heavily rely on three-dimensional (3D) imaging data. Benefits include improved operator ergonomics, reduced fatigue, and simplified hand–eye coordination. Head-mounted AR displays may hold great potential for enhancing surgical navigation given their compactness and intuitiveness of use. In this work, the authors propose a method that can intra-operatively locate bone structures using tracked ultrasound (US), registers to the corresponding pre-operative computed tomography (CT) data and generates 3D AR visualisation of the operated surgical scene through a head-mounted display. The proposed method deploys optically-tracked US, bone surface segmentation from the US and CT image volumes, and multimodal volume registration to align pre-operative to the corresponding intra-operative data. The enhanced surgical scene is then visualised in an AR framework using a HoloLens. They demonstrate the method's utility using a foam pelvis phantom and quantitatively assess accuracy by comparing the locations of fiducial markers in the real and virtual spaces, yielding root mean square errors of 3.22, 22.46, and 28.30 mm in the x, y, and z directions, respectively.

1. Introduction: Minimally invasive orthopaedic surgical procedures greatly benefit from computer-assisted, image-based, navigation and guidance to improve surgical accuracy and enable minimally invasive surgery [1–3]. Current surgical navigation systems typically display available imaging data on a conventional two-dimensional (2D) computer screen located away from the physical, real-world operated scene. This presents several challenges for the surgeon who cannot observe the computer screen and surgical site simultaneously, potentially increasing the risk of error. Furthermore, the challenging mental exercise needed to map screen-displayed 2D information to the corresponding 3D real world anatomy can be especially problematic for new or less experienced surgeons. Augmented reality (AR) technologies thus provide a safe approach to intuitively augment the operator's view of the scene with fused and complex 3D information not accessible by human vision. More specifically, head-mounted AR displays are especially useful for such applications since their compact size and simple integration into the surgical environment and workflow allows the surgeon to maintain uninterrupted gaze on the operated scene, enables a potential reduction in surgical time, and improved operator ergonomics [4].

Several recent studies examined the use of HMDs in surgery. In the closest work to ours, Hajek *et al.* [5] presented a method for locating bone using a HoloLens mounted on a C-arm fluoroscope that communicates with another HoloLens worn by the user for percutaneous orthopaedic interventions. The authors used a markerless setup based on simultaneous localisation and mapping. Chen *et al.* [6] presented a system based on a different head-mounted display (HMD), the nVisor ST60, for overlaying a hologram of a pelvis model over itself. They tracked the HMD with a stereo optical tracker and used a tracked stylus for locating the pelvis. Vassalo *et al.* [7] examined the stability of the HoloLens. In that study, the authors digitised several points on a hologram with an optically-tracked stylus as seen by a spectator through the HoloLens and examined the effect of user movement or sensor occlusion in several scenarios on the stability of these points. That work's focus was on stability, but not accuracy; in other words, the hologram position was compared relative to itself at different times, but the absolute position was not measured with respect to the environment. Pratt *et al.* [8] used the HoloLens to 'see through' the patient's skin to visualise patients' vasculature in the pre-operative stage of lower extremity reconstructive surgery. Manual registration by surgeon hand gestures was used to register the hologram over the real anatomy. The device was tested in several surgical cases. Khuzagliyev *et al.* [9] presented a method for guiding a needle using tracked ultrasound (US) and visualising holographic guides over the needle using the HoloLens.

These papers presented methods for anatomy localisation using either manual registration or traditional X-ray based imaging techniques. In surgery, automatic registration of pre- and intra-operative data is desirable as manual registration data increases operating times significantly and is error prone [10]. Further, X-ray-based imaging methods expose the patients and surgeons to significant amounts of ionising radiation [11]. There remains a gap in the literature for head-mounted AR systems that use automatic, non-ionising imaging modalities for bone localisation.

Recently, US has been proposed as a non-ionising, viable alternative to intra-operative X-ray for bone localisation in navigated procedures. Bone surface detection with the US has been studied extensively over the last two decades, with one of the first studies dating back as far as 2001 [10]. However, automatic segmentation of the bone surface in the intra-operative US and subsequent multimodal registration to pre-operative computed tomography (CT) presented a significant challenge. Several studies have since attempted to address this challenge by implementing automatic US segmentation and US-to-CT registration algorithms. Hacihaliloglu *et al.* used phase symmetry features for automatic bone surface segmentation and fracture detection [12], as well as US-to-CT bone surface registration with Gaussian mixture modelling [13]. More recently, Pandey *et al.* proposed a faster and more robust method for 3D US-to-CT registration that

uses shadow peak (SP) bone surface segmentation in the US and normalised cross correlation (NCC) registration [14].

In this Letter, we present a method that locates bone in a known reference frame from intra-operative US images, aligns that to the corresponding bone from pre-operative CT images, with the fused 3D imaging information aggregated and displayed within a head-mounted AR visualisation of the surgical scene. For AR visualisation we use the HoloLens (Microsoft® Corporation, Redmond, WA, USA) optical see-through HMD for being a self-contained device and readily available in the market. The HoloLens is a stand-alone wearable holographic computer in the form of a smart HMD that is equipped with a central processing unit (CPU), an array of environment-sensing cameras, time-of-flight depth sensors, inertial measurement unit, and holographic processing unit for processing the multimodal data from the sensors without overloading the CPU, a battery, and waveguides for displaying holograms. For the US to CT bone surface segmentation and registration, we use SP segmentation and NCC registration as described by Pandey *et al.* [14] for being relatively less computationally intensive and more robust. We demonstrate our pipeline on a pelvis US phantom.

$$ {}^{\mathrm{CT}}T_{\mathrm{Patient}} = {}^{\mathrm{CT}}T_{\mathrm{US}}\,{}^{\mathrm{US}}T_{\mathrm{Probe}}\,{}^{\mathrm{Probe}}T_{\mathrm{Tracker}}\,{}^{\mathrm{Tracker}}T_{\mathrm{Common}}\,{}^{\mathrm{Common}}T_{\mathrm{Patient}} \quad (1) $$

2. Methods: To overlay a CT model with the real scene, we need to find the transformation from the CT frame to the AR frame, ${}^{\mathrm{CT}}T_{\mathrm{Patient}}$, and this is realised through a chain of transformations by using an optical tracker, tracked the US and a custom-built dual tracking (optical and AR) structure (Fig. 1). The transforms are listed in (1), where ${}^{\mathrm{US}}T_{\mathrm{Probe}}$ and ${}^{\mathrm{Common}}T_{\mathrm{Patient}}$ are obtained through pre-calibration, and ${}^{\mathrm{CT}}T_{\mathrm{US}}$ is obtained through registration.

2.1. Pre-operative imaging and segmentation: In navigated surgery, a scan of the bony anatomy is acquired pre-operatively for planning and intra-operative display, often by CT. Similarly, we acquired a CT volume of the pelvis model for display on the HoloLens, using a CT750HD (General Electric, Boston, MA, USA) scanner. The CT volume was exported in Digital Imaging and Communications in Medicine (DICOM) format with $0.59 \times 0.59 \times 0.625$ mm voxel spacing. For display on the HoloLens, we first segmented and converted the volumetric CT data to a mesh surface model. We did this in 3D Slicer [15] by first segmenting and removing the CT table by manual mouse manipulation. Then we used manual intensity thresholding to remove all low-intensity unwanted artefacts. We converted the segmented volume to a mesh surface model in 3D Slicer and exported as a mesh surface file for importing into Unity (ver. 2017.2.0f3).

2.2. Tracking: Intra-operatively, a HoloLens-trackable printed photograph is attached rigidly to the pelvis, and we refer to this as the Patient reference frame. This target is tracked by the HoloLens front-facing webcam using Vuforia (PTC Inc., Needham, MA) software development kit. For AR display, we locate the pelvis in the patient reference frame, or in other words, we compute the transform ${}^{\mathrm{CT}}T_{\mathrm{Patient}}$ using the optically-tracked US. The MicrUS-L12 (Telemed, Vilnius, Lithuania) US probe is tracked with the Polaris Vega (Northern Digital Inc., Waterloo, ON, Canada) optical tracker. We equip the US probe with a dynamic reference frame (DRF), a set of reflective spheres on a rigid body that is trackable by the Vega. We use PLUS [16] to receive and combine tracking and imaging data from the optical tracker and US probe, and send this data in real-time to 3D Slicer over OpenIGTLink [17]. We use a tracked stylus for calibrating the system. We first determine the stylus tip to stylus calibration, ${}^{\mathrm{Tip}}T_{\mathrm{Stylus}}$, with pivot calibration. To calculate the US image to probe transformation, ${}^{\mathrm{US}}T_{\mathrm{Probe}}$, we use the Polaris stylus calibration method as described by Hsu *et al.* [18], by moving the stylus tip to multiple positions in the US scan plane while simultaneously tracking it in the probe reference frame, then solving for the rigid transform with iterative closest point (ICP)-based registration. These calibrations were performed in Slicer.

The US and HoloLens reference frames are resolved using a common target that is identifiable by both the Vega and the HoloLens camera. For this, we designed and fabricated the common reference frame (please refer to Fig. 2) which is a jig that combines the printed photograph and a custom Vega-trackable DRF, printed from the I-STAR library of DRFs [19]. We calibrated the patient reference frame to this DRF (${}^{\mathrm{Common}}T_{\mathrm{Patient}}$) using the same stylus and ICP calibration method that was used for calibrating the US image to the probe DRF, but replacing the US image with the printed photograph (patient), and replacing Probe DRF with Common DRF, in Slicer.

2.3. Intra-operative US acquisition: To locate the pelvis with respect to the patient reference frame, we obtained a tracked US volume of the pelvis in the patient reference frame. We

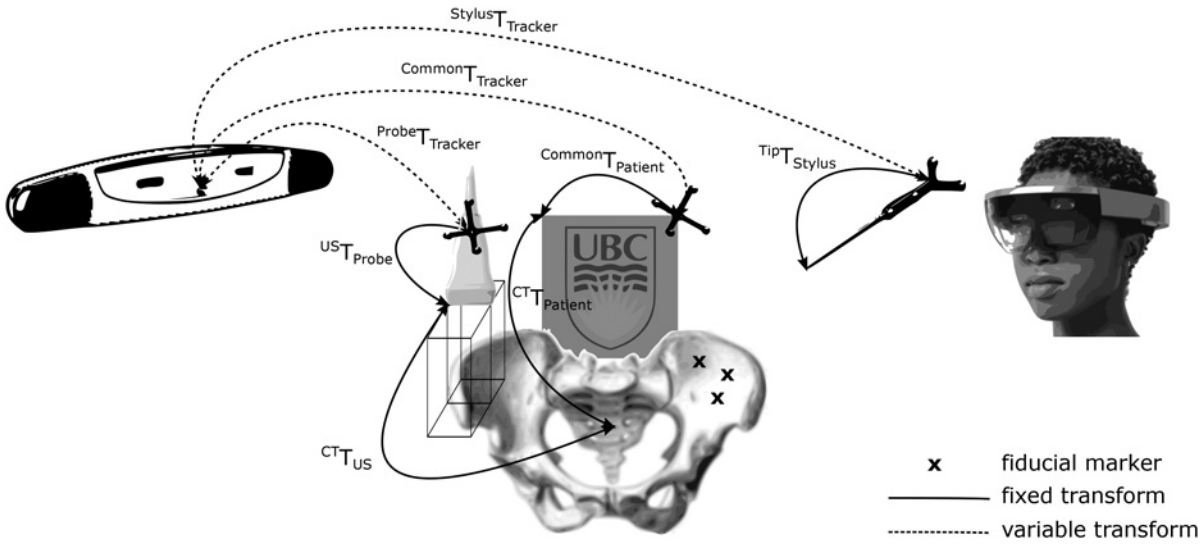

Fig. 1 *Overview of the HoloLens-based AR system showing the transformations between the different components of the system*

doi: 10.1049/htl.2018.5061

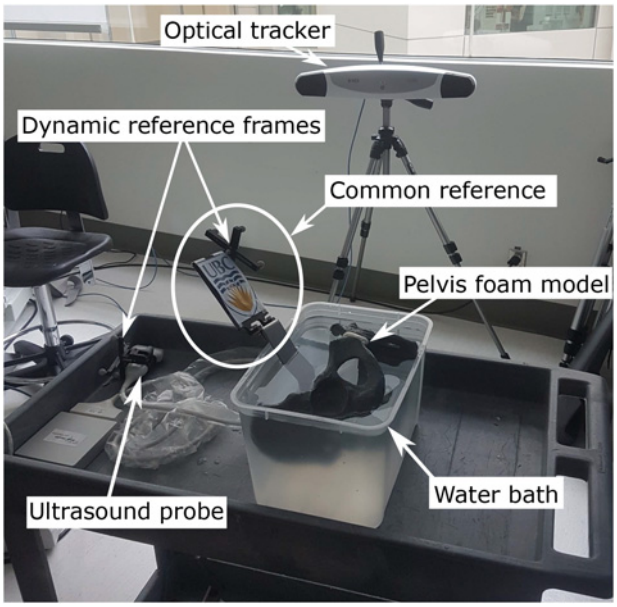

Fig. 2 *US acquisition set-up showing the optical tracker, US probe, and foam pelvis model submerged in a water bath*

submerged the pelvis in water for US acquisition (see Fig. 2). We set the US probe to 10 MHz frequency and depth of 70 mm. We collected 2691 tracked US frames and reconstructed the volume using a pixel-based method with hole-filling. We used 1 mm voxel spacing, trilinear interpolation for pixel distribution, and mean compounding for overlapping pixels. For hole-filling, we used a Gaussian-weighted element with three-voxel diameter and two-voxel standard deviation (see resulting volume in Figs. 3*a* and *g*).

2.4. Bone segmentation and CT to US registration: To compute ${}^{CT}T_{US}$ we use SP segmentation, inverse distance map transform, and NCC-based registration as described by Pandey *et al.* [14] (see Fig. 3). Before applying this algorithm, pre-processing steps were required due to the differences between this study and the study by Pandey *et al.*, namely using a different US probe and using water instead of agar as the US medium. For the US, we apply manual intensity thresholding to overcome the artefacts from the Telemed system's time gain compensation, which did not allow for a sufficient acoustic shadow to be cast. For CT, we use the same volume that was pre-operatively segmented, but we further apply manual intensity thresholding to remove the very high intensity signals from the brass screws.

After pre-processing the volume, we applied the steps as described by Pandey *et al.* We used SP to automatically segment

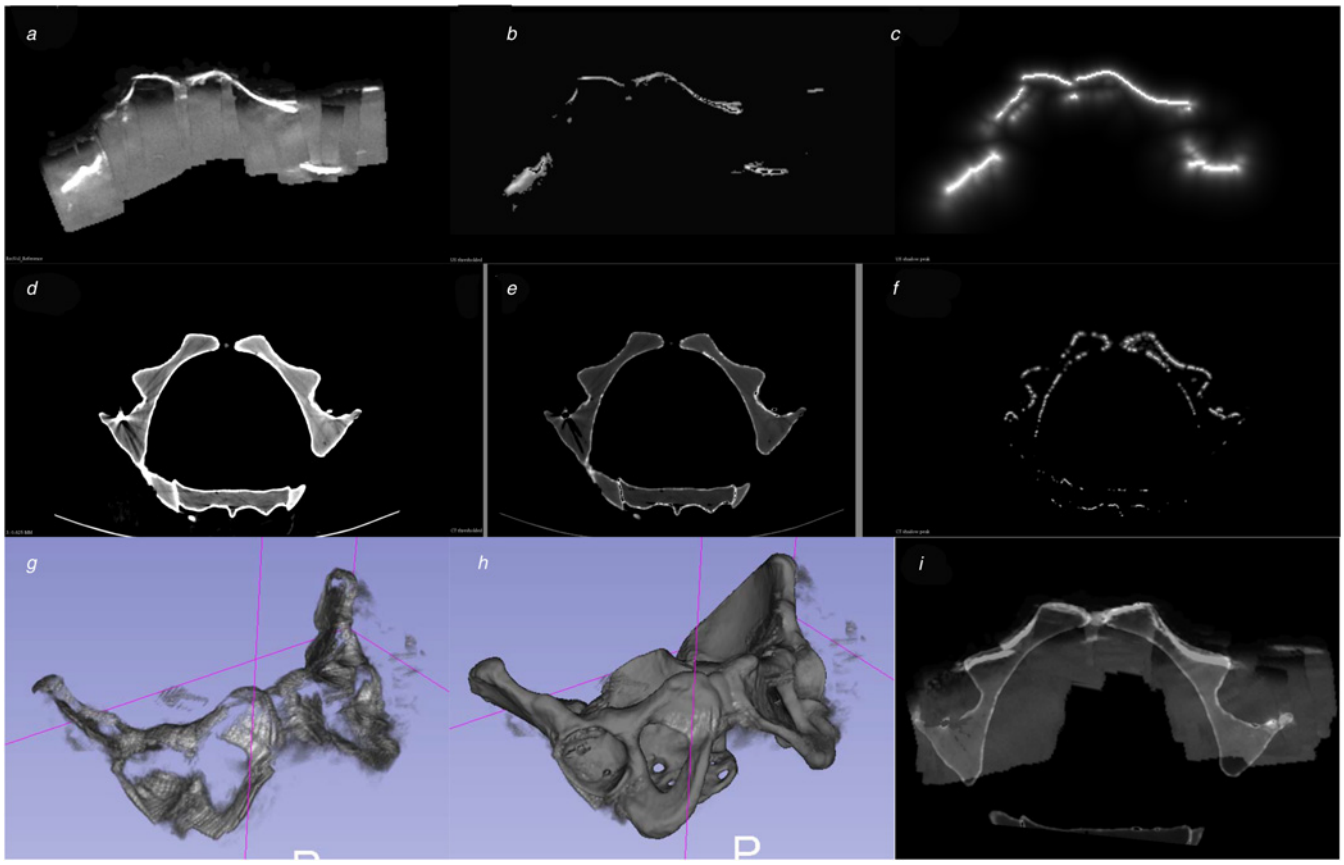

Fig. 3 *CT to US registration steps*
a Axial slice of 3D US volume
b US volume after thresholding
c Distance map of thresholded US volume after applying SP segmentation algorithm
d Axial slice of CT volume
e CT after thresholding
f Distance map of thresholded CT volume after applying SP algorithm
g 3D view of the volume rendering of 3D US volume in slicer
h 3D view of pelvis model, segmented from the CT volume, registered to the US volume
i Axial view of registered CT and US volumes overlaid

bone surfaces, based on bone shadowing and maximum pixel intensities, in both the US volume reconstruction and CT volumes (see Fig. 3). We used the nonlinear inverse distance transform to improve convergence of the intensity-based 3D registration between the US and virtual CT volumes, which is achieved by maximising the NCC between the 3D images using stochastic gradient descent. We thus could calculate the transform ${}^{CT}T_{US}$. The segmentation and registration algorithms were incorporated into the 3D Slicer framework using elastix [20] and MATLAB bridging modules.

2.5. Accuracy validation: To assess the total registration error (TRE) of the system, we placed 12 fiducials in the form of brass screws in the surface of the pelvis model. Due to their metallic nature, we simply segmented the fiducials in CT using manual intensity thresholding and then converted to a mesh surface in 3D Slicer. We applied the ${}^{CT}T_{Patient}$ to this mesh. We imported the transformed mesh into unity for display on the HoloLens. We digitised the locations of the brass screw heads in the patient reference frame with the tracked stylus. Similarly, we digitised the corresponding virtual screw heads as seen through the HoloLens (see Fig. 4) with the tracked stylus in the patient reference frame. We collected ten points for each virtual screw by moving the stylus away from and back towards the head of the virtual fiducial and considered the location of each virtual fiducial to be the centroid of all points collected from that fiducial. We calculated the TRE as in (2), where v_i refers to the location of a virtual fiducial (i.e. the red virtual screw as seen through the HoloLens in Fig. 3) in the patient reference frame, r_i refers to the corresponding location of the real fiducial (i.e. the real screw) in the patient reference frame, and n represents the total number of fiducials

$$\mathrm{TRE} = \sqrt{\frac{\sum_{i=1}^{n}\left((v_{ix}-r_{ix})^2+(v_{iy}-r_{iy})^2+(v_{iz}-r_{iz})^2\right)}{n}}. \quad (2)$$

3. Results and discussion: We simulated a Computer Assisted Orthopaedic Surgery (CAOS) scenario with AR visualisation by overlaying a hologram of a pelvis foam model over the real foam model as shown in Fig. 4. To assess the TRE of the system, or in other words, how well the virtual hologram is registered to the real pelvis, we measured the locations of the real and virtual fiducials with a tracked stylus. The measured locations are shown in a 3D plot (Fig. 5). We measured a TRE of 36.90 mm, as described in (2), with x, y, and z components of 3.22, 22.46, and 28.30 mm, respectively.

Our preliminary results are promising, but with room for improvement. One of the limitations of our system currently is the use of a trackable printed target attached to the bone, which can be considered intrusive to the surgical site. With future improvements, our system may be modified such that this target can be situated separately from the patient and does not have to be attached to the bone at all. This would require real-time US acquisition, segmentation, and registration such that bone location can be quickly determined if the bone moves.

Furthermore, we observed some limitations of the HoloLens' capability for displaying holograms. Most notably, the observed field-of-view of the HoloLens is relatively narrow, such that parts of the hologram would disappear if the user's head drifted too far

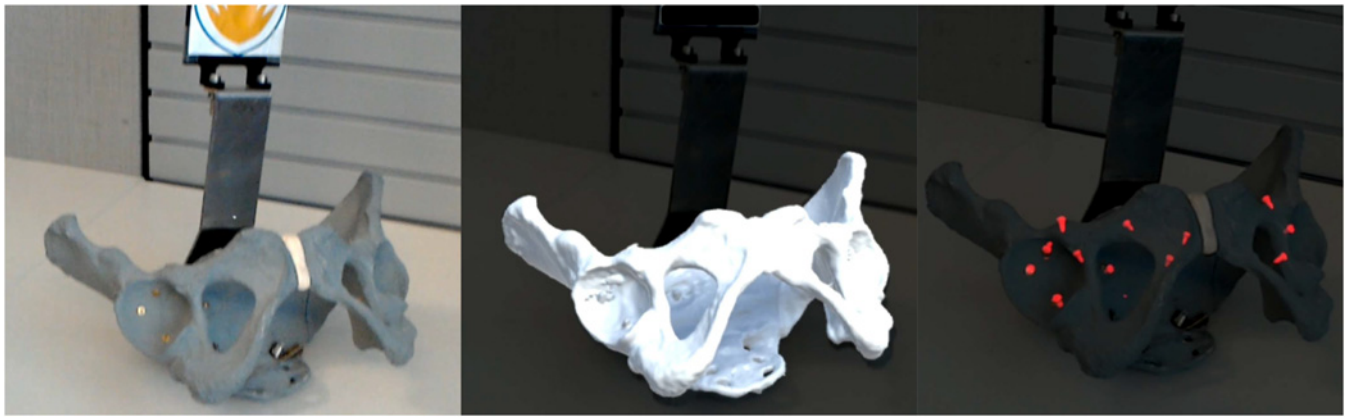

Fig. 4 *HoloLens spectator view showing the real pelvis foam model (left), the same model with virtual pelvis overlay (middle), and the same model with virtual fiducials overlay (right)*

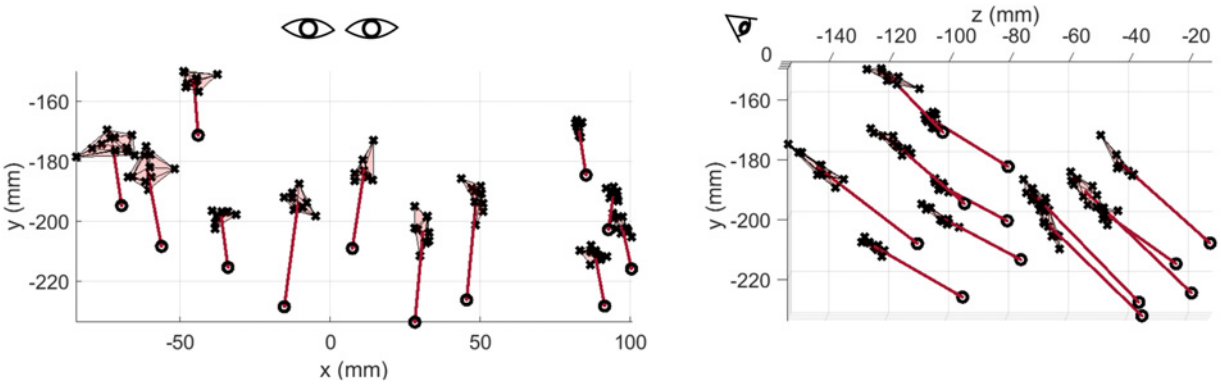

Fig. 5 *Real versus virtual fiducials in the patient reference frame in the x–y (left) and y–z (right) views. Eyes are drawn to represent the spectator's line-of-sight. The real fiducials are represented by a circle each. The virtual fiducials are represented each by a cluster of crosses. Each cross represents a sample point acquired by the user. An arrow connects each real fiducial to its corresponding virtual counterpart at the centroid of the cluster*

up or down. This detracts from the illusion of the hologram. In digitising the fiducials, it was easy to feel and locate the brass screw heads with the tracked stylus, but it was not easy to locate the same points on the holograms of the screws (see Fig. 4). This is because the holograms rendered by the HoloLens are not true holograms, in that they are displayed directly in front of the user's view on the waveguides, so the stylus does not occlude the screws when positioned in the line-of-sight between the user's eyes and hologram. This confuses the user's perception about the true depth of the hologram and leaves the user to rely mainly on size, focus, and parallax cues to estimate depth. This difficulty in depth perception is apparent when looking at the spread of each cluster of points taken by the user of each virtual fiducial, which is the greatest in the direction of the user's line-of-sight (see Fig. 5).

The reported accuracy is currently not acceptable in terms of surgical application, but on par with the findings of other papers for the HoloLens. For example, the closest study by Hajek *et al.* [5] found a calibration root-mean-squared error of 26.6 mm, with component errors in the x, y, and z directions of 4.10, 3.02, and 43.18 mm, respectively, as well as a TRE of 11.46 mm. We observed a similar pattern in our component errors in the x, y, and z directions of 3.22, 22.46, and 28.30 mm, respectively. Note the largest errors are in the y and z directions. We suspect that this error is due to the fact that the patient reference frame printed marker was placed relatively far away from the pelvis, so small rotational tracking errors are magnified farther away from the printed marker. No other papers reported quantitative accuracy measurements for the HoloLens as far as we know. However, one study that used the nVisor ST60 for head-mounted AR visualisation, and used a stereo optical tracker for tracking the nVisor, reported a mean distance error of 0.809 mm ± 0.05 mm and mean angular error of 1.038° ± 0.05° [6].

Future work will involve improving accuracy, potentially by improving the design of the tracking system, e.g. by replacing the single camera on the HoloLens with a stereo system that can measure the depth more accurately, or by using the raw data from the HoloLens depth sensors if access is provided by the manufacturer, or by using a separate optical tracker set-up such as the one used by Chen *et al.* [6]. If accuracy can be significantly improved, the next steps in this study would be the real-time integration of the pipeline with an HMD. Furthermore, the system must be tested on more realistic US phantoms that use materials other than water and foam, before a clinical study can be conducted.

4. Conclusion: We proposed a method for AR display in CAOS that uses intra-operative tracked US to locate bone and register to it pre-operative CT data. We successfully demonstrated our method on a foam pelvis model with a HoloLens for AR display and quantitatively measured the total system accuracy. With improvements to accuracy, our methods may be used with head-mounted AR displays to enhance the operator's experience in CAOS procedures and provide a non-ionising alternative to intra-operative X-ray bone localisation. Future work will focus on improving the accuracy of this system to a level that may enable clinical translation.

5. Funding and declaration of interests: This work was funded by the Natural Sciences and Engineering Research Council (grant no. CHRP 478466-15) and the Canadian Institutes of Health Research (grant no. CPG-140180).

6. Conflict of interest: None declared.

7 References

[1] Sugano N.: 'Computer-assisted orthopedic surgery', *J. Orthop. Sci.*, 2003, **8**, pp. 442–448

[2] Cleary K., Peters T.M.: 'Image-guided interventions: technology review and clinical applications', *Annu. Rev. Biomed. Eng.*, 2010, **12**, pp. 119–142

[3] Joskowicz L., Hazan E.J: 'Computer aided orthopaedic surgery: incremental shift or paradigm change?', *Med. Image Anal.*, 2016, **33**, pp. 84–90

[4] Yoon J.W., Chen R.E., Kim E.J., *ET AL.*: 'Augmented reality for the surgeon: systematic review', *Int. J. Med. Robot. Comput. Assist. Surg.*, 2018, **14**, (4), pp. 1–13

[5] Hajek J., Unberath M., Fotouhi J., *ET AL.*: 'Closing the calibration loop: an inside-out-tracking paradigm for augmented reality in orthopedic surgery', Med. Image Comput. Comput. Assist. Interv., Grenada, Spain, 2018

[6] Chen X., Xu L., Wang Y., *ET AL.*: 'Development of a surgical navigation system based on augmented reality using an optical see-through head-mounted display', *J. Biomed. Inf.*, 2015, **55**, pp. 124–131

[7] Vassalo R., Ranken A., Chen E., *ET AL.*: 'Hologram stability evaluation for Microsoft HoloLens'. Proc. SPIE, Orlando, Florida, United States, 2017, vol. 10136

[8] Pratt P., Ives M., Lawton G., *ET AL.*: 'Through the HoloLens looking glass: augmented reality for extremity reconstruction surgery using 3D vascular models with perforating vessels', *Eur. Radiol. Exp.*, 2018, **2**, pp. 1–7

[9] Kuzhagaliyev T., Clancy N.T., Janatka M., *ET AL.*: 'Augmented reality needle ablation guidance tool for irreversible electroporation in the pancreas'. Proc. SPIE, Houston, Texas, United States, 2018, vol. 10576

[10] Tonetti J., Carrat L., Blendea S., *ET AL.*: 'Clinical results of percutaneous pelvic surgery. Computer assisted surgery using ultrasound compared to standard fluoroscopy', *Comput. Aided Surg.*, 2001, **6**, pp. 204–211

[11] Ecker T., Jost J., Cullman J., *ET AL.*: 'Percutaneous screw fixation of the iliosacral joint: a case-based preoperative planning approach reduces operating time and radiation exposure', *Injury*, 2017, **48**, pp. 1825–1830

[12] Hacihaliloglu I., Abugharbieh R., Hodgson A.J., *ET AL.*: 'Automatic bone localization and fracture detection from volumetric ultrasound images using 3-D local phase features', *Ultrasound Med. Biol.*, 2012, **1**, pp. 128–144

[13] Hacihaliloglu I., Brounstein R., Guy P., *ET AL.*: '3D ultrasound-CT registration in orthopaedic trauma using GMM registration with optimized particle simulation-based data reduction'. Medical Image Computing and Computer Assisted Interventions, Nice, France, 2012 (*LNCS*, **7511**), Part II, pp. 82–89

[14] Pandey P., Guy P., Hodgson A.J., *ET AL.*: 'Fast and automatic bone segmentation and registration of 3D ultrasound to CT for the full pelvic anatomy – a comparative study', *Int. J. Comput. Assist. Radiol. Surg.*, 2018, doi: 10.1007/s11548-018-1788-5

[15] Kikinis R., Pieper S.D., Vosburgh K.: '3D slicer: a platform for subject-specific image analysis, visualization, and clinical support', in Jolesz F.A. (Ed.): '*Intraoperative Imaging and Image-Guided Therapy*', (Springer, New York, 2014, 1st ed.), pp. 277–289

[16] Lasso A., Heffter T., Rankin A., *ET AL.*: 'Plus: opensource toolkit for ultrasound-guided intervention systems', *IEEE Trans. Biomed. Eng.*, 2014, **61**, pp. 2527–2537

[17] Tokuda J., Fischer G., Papademetris S., *ET AL.*: 'Openigtlink: an open network protocol for image-guided therapy environment', *Int. J. Med. Robot. Comput. Assist. Surg.*, 2009, **5**, pp. 423–434

[18] Hsu P., Treece G.M., Prager R.: 'Comparison of freehand 3-D ultrasound calibration techniques using a stylus', *Ultrasound Med. Biol.*, 2008, **34**, pp. 1610–1621

[19] Brown A., Uneri A., Silva T.D.: 'Design and validation of an open-source library of dynamic reference frames for research and education in optical tracking', *J. Med. Imaging*, 2018, **5**, pp. 5–8

[20] Klein S., Staring M., Murphy M.A., *ET AL.*: 'Elastix: a toolbox for intensity-based medical image registration', *IEEE Trans. Med. Imaging*, 2010, **29**, pp. 196–205